Population inversion by chirped pulses

Tianshi Lu

Phys. Rev. A **84**, 033411 — Published 13 September 2011

DOI: 10.1103/PhysRevA.84.033411

Population inversion by chirped pulses

Tianshi Lu[1]
[1]Dept. of Mathematics and Statistics, Wichita State University
Wichita, KS 67260-0033 USA

August 17, 2011

Abstract

In this paper we analyze the condition for complete population inversion by a chirped pulse over a finite duration. The nonadiabatic transition probability is mapped in the two dimensional parameter space of coupling strength and detuning amplitude. Asymptotic forms of the probability are derived by the interference of nonadiabatic transitions for sinusoidal and triangular pulses. The qualitative difference between the maps for the two types of pulses is accounted for. The map is used for the design of stable inversion pulses under specific accuracy thresholds.

1 Introduction

Population transfer between energy levels with time-dependent coupling has been studied for many decades. From the pioneering works on the linear-crossing model by Landau [1] and Zener [2] to the adiabatic rapid passage in magnetic resonance [3], it has been shown in many literatures that with a slow level crossing the state follows instantaneous energy eigenstate adiabatically. In the adiabatic limit where the level crossing is infinitely slow, a complete population inversion of a two-level system can be realized, provided that the energy eigenstates are switched by the time-dependent coupling. For faster level crossings, the population inversion can be incomplete due to nonadiabatic transitions. We denote the probability for not making the desired adiabatic transition as P_{nad}.

Most literatures on level crossing models investigated single population transfers, which could be modelled by infinite-time processes. Transition of finite duration has been studied by, eg., Vitanov and Garraway [4], Bateman and Freegarde [5]. In a recent laser experiment by Miao et. al. [6], helium atoms subject to a sequence of counterpropagating chirped light pulses underwent multiple adiabatic rapid passages. The coherent exchange of momentum between pairs of counterpropagating light pulses produced large optical forces. The optical force was proportional to the population transfer over each light pulse. The application of periodic light pulses make it necessary to use finite-time level crossing models to calculate the population transfer. The nonadiabatic transition probability P_{nad} for various finite-time level crossing models was studied numerically in Ref. [7], and an approximate formula for P_{nad} was derived using a perturbation method in Ref. [8]. It was shown in Ref. [8] that the distributions of P_{nad} for finite-time models in the parameter space of the Hamiltonian were qualitatively different from those for infinite-time models, such as the Landau-Zener model and the Demkov-Kunike model [9].

The general form of a time-dependent Hamiltonian for a two-level system (see Ref. [10]) is,

$$\mathcal{H}_0(t) = \frac{\hbar}{2}\begin{pmatrix} \delta(t) & \Omega(t) \\ \Omega(t) & -\delta(t) \end{pmatrix}. \tag{1.1}$$

If we take the electric dipole interaction between the light and atoms as an example, in the frame that rotates at the frequency of the light field, $\delta(t)$ would be the detuning of the light frequency from the atomic resonance, and $\Omega(t)$ would be the Rabi frequency [11]. In an infinite-time model, the transition is from $t = -\infty$ to $t = \infty$, and the coupling $\Omega(t)$ never vanishes. For example, in the Landau-Zener (LZ) model,

$$\Omega(t) = b, \quad \delta(t) = at; \tag{1.2}$$

and in the Demkov-Kunike (DK) model,

$$\Omega(t) = \Omega_0 \mathrm{sech}(\frac{\pi t}{2\tau}), \quad \delta(t) = \delta_0 \tanh(\frac{\pi t}{2\tau}). \tag{1.3}$$

In a finite-time pulse model, the transition is from $t = -T/2$ to $t = T/2$, where T is the duration of the coupling. We denote the maximums of $\delta(t)$ and $\Omega(t)$ by δ_0 and Ω_0 respectively. The constant pulse model, or the finite Landau-Zener model, in which

$$\Omega(t) = \Omega_0, \quad \delta(t) = \delta_0 \frac{2t}{T}, \tag{1.4}$$

has been studied extensively by Vitanov and Garraway [4]. In this paper, we will study pulses that continuously vanish at the beginning and the end of the finite duration. Typical examples are the sinusoidal pulse model [6],

$$\Omega(t) = \Omega_0 \cos\omega_m t, \quad \delta(t) = \delta_0 \sin\omega_m t, \tag{1.5}$$

where $\omega_m = \pi/T$, the triangular pulse model [8],

$$\Omega(t) = \Omega_0(1 - \frac{2|t|}{T}), \quad \delta(t) = \delta_0 \frac{2t}{T}. \tag{1.6}$$

Assuming that δ_0 and Ω_0 can be scaled independently as in the experiment by Miao et al. [6], we can map P_{nad} in the two dimensional parameter space of normalized δ_0 and Ω_0, as shown in Fig. 1 for sinusoidal and triangular pulses. In contrast to the asymptotic method proposed by Dykhne [12] and Davis and Pechukas [13] for infinite-time models and its generalization to multiple singularities in the complex t plane [14], which claimed that P_{nad} depends only on the energy sheets (via their continuation into the complex t plane), P_{nad} for finite-time models is not only determined by the eigenenergies, but also by the time dependence of $\delta(t)$ and $\Omega(t)$. The problem of interest is how the pulse profile and parameters affect P_{nad}, and in particular, how to achieve a stable inversion, ie, $P_{nad} = 0$.

For $\Omega_0 T \gg 1$ and/or $\delta_0 T \gg 1$, it is more advantageous to work in the rotating adiabatic frame [8], in which the Hamiltonian is

$$\mathcal{H}(t) = \frac{\hbar}{2}\begin{pmatrix} 0 & i\dot{\theta}(t)e^{is(t)} \\ -i\dot{\theta}(t)e^{-is(t)} & 0 \end{pmatrix}, \tag{1.7}$$

where $0 \le \theta \le \pi$ with $\tan\theta(t) = \Omega(t)/\delta(t)$, and $s(t) = \int_0^t \Omega'(\tau)d\tau$ with $\Omega'(t) = \sqrt{\Omega^2(t) + \delta^2(t)}$. Denote the propagation matrix in the rotating adiabatic frame from 0 to t and from $-t$ to 0 by

$$O(t) = \begin{pmatrix} \alpha^*(t) & -\beta(t) \\ \beta^*(t) & \alpha(t) \end{pmatrix}, \quad O(-t) = \begin{pmatrix} \alpha^*(-t) & -\beta(-t) \\ \beta^*(-t) & \alpha(-t) \end{pmatrix}. \tag{1.8}$$

If the pulse is symmetric in the sense that $\delta(-t) = -\delta(t)$, $\Omega(-t) = \Omega(t)$, by time reversal we have

$$\alpha(-t) = \alpha(t), \quad \beta(-t) = \beta^*(t). \tag{1.9}$$

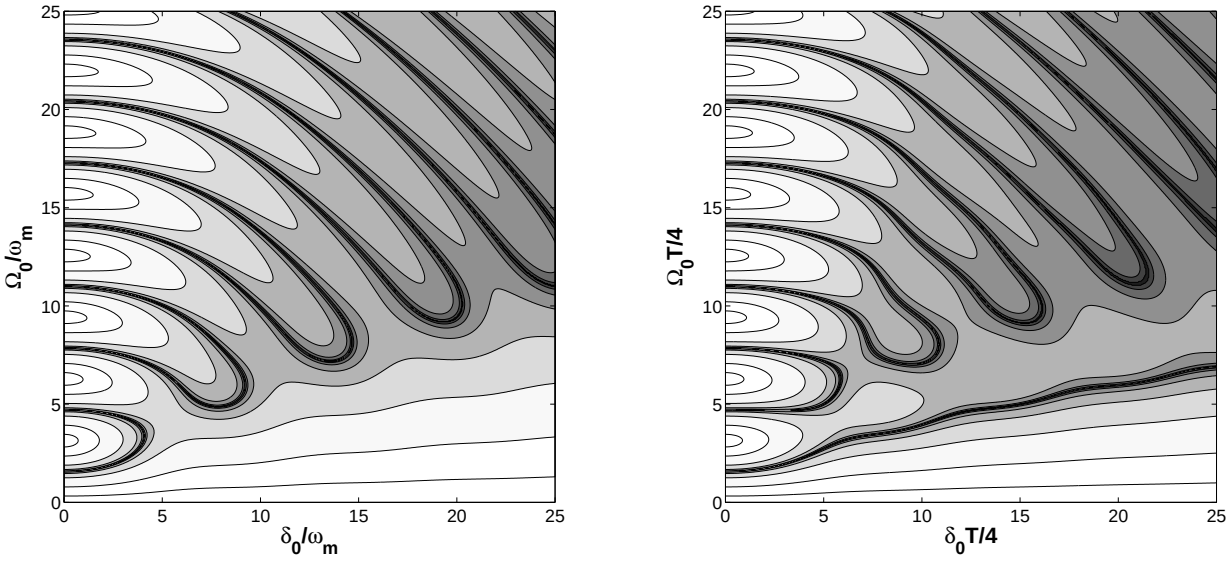

(a) Sinusoidal Pulse

(b) Triangular Pulse

Figure 1: Map of P_{nad} in the pulse parameter space. The curves are for $P_{nad} = 0.9, 0.5, 0.1, 0.01, 0.001, ...$ The darkest regions are for vanishing P_{nad}.

Denote the propagation matrix in the rotating adiabatic frame over the entire pulse by

$$O_{ad} = O(T/2)O(-T/2) = \begin{pmatrix} \alpha_{ad}^* & -\beta_{ad} \\ \beta_{ad}^* & \alpha_{ad} \end{pmatrix}. \tag{1.10}$$

For pulse profiles with adiabatic states at the end of the pulse inverted from those at the beginning of the pulse, such as sinusoidal or triangular pulses,

$$P_{nad} = |\beta_{ad}|^2, \quad \beta_{ad} = \alpha(-T/2)\beta(T/2) + \beta(-T/2)\alpha^*(T/2).$$

For a symmetric pulse, β_{ad} is a real number, and

$$P_{nad} = \beta_{ad}^2 = (\alpha(T/2)\beta(T/2) + \alpha^*(T/2)\beta^*(T/2))^2, \tag{1.11}$$

which implies that the traces of $P_{nad} = 0$ in the map are curves (cf. Fig. 1); while for a nonsymmetric pulse profile, β_{ad} is complex and the traces of $P_{nad} = 0$ in the map are scattered points. Since we are interested in stable inversions, we will only consider symmetric pulses.

As shown in Fig. 1, the maps of P_{nad} for finite-duration pulses are divided into oscillatory and nonoscillatory regions. In the nonoscillatory region, the nonadiabatic transition is dominated by the Landau-Zener transition at resonance, which gives

$$P_{nad} \cong e^{-4\pi k_1}, \tag{1.12}$$

where $k_1 = \Omega_0^2/(8\dot{\delta}_0)$. The factor of 8 is introduced for convenience (see Appendix A). In the oscillatory region, the phase of oscillation depends on the area swept by the difference between the eigenenergies over the pulse duration. Let

$$s_0 = \int_{-T/2}^{T/2} [E_+(t) - E_-(t)]dt, \tag{1.13}$$

where $E_\pm = \pm\frac{\hbar}{2}\sqrt{\Omega^2(t) + \delta^2(t)}$ are the eigenenergies of the Hamiltonian in Eq. (1.1). For non-chirped pulses, the area theorem [11] states that

$$P_{nad} = \cos^2(\frac{s_0}{2}). \tag{1.14}$$

Non-chirped inversion pulses require $s_0 = (2n+1)\pi$. In the adiabatic limit, by the first order perturbation in the rotating adiabatic frame [8],

$$P_{nad} \cong (\frac{\dot{\Omega}_0}{\delta_0^2})^2 \sin^2(\frac{s_0}{2}). \tag{1.15}$$

Adiabatic inversion pulses require $s_0 = 2n\pi$. We will explain the change from $s_0 = (2n+1)\pi$ for non-chirped inversion pulses to $s_0 = 2n\pi$ for adiabatic inversion pulses in Section 2.

Finite-duration chirped pulses can be compared with the Demkov-Kunike model and finite Landau-Zener model. The maps of P_{nad} for all these models consist of oscillatory and nonoscillatory regions. However, the oscillations for different models have distinct characteristics. The Demkov-Kunike model is exactly solvable [19]. In the oscillatory region, $P_{nad}^{DK} = \cos^2\tau\sqrt{\Omega_0^2 - \delta_0^2}/\cosh^2\tau\delta_0$. The condition for population inversion is $\tau\sqrt{\Omega_0^2 - \delta_0^2} = (n+\frac{1}{2})\pi$, rather than determined by the phase s_0. The finite Landau-Zener model differs from sinusoidal and triangular pulses in that the pulse in the finite Landau-Zener model does not vanish continuously at the ends of the duration. By the analysis of Vitanov and Garraway [4], the condition for the population inversion is $s_0 = (2n+1)\pi$ throughout the oscillatory region.

The map of P_{nad} for sinusoidal pulses also differs from that for triangular pulses. In Fig. 1(a), the trace of sinusoidal pulses with population inversion consists of a sequence of loops; while in Fig. 1(b), the trace of triangular pulses with inversion has an extra curve below the loops. In Section 3, we will explain this difference using a split level crossing model. In Section 4 the model is extended for the stability analysis of adiabatic and nonadiabatic inversion pulses.

2 Oscillation phase of P_{nad}

In the oscillatory region of the map, $\Omega_0 \gg \delta_0$, the nonadiabatic transition is dominated by the avoided crossing at the two ends of the duration. The pulse from 0 to $T/2$ can be regarded as the half LZ transition from $-\infty$ to 0 with adiabaticity $k_2 = \delta_0^2/(8\dot{\Omega}_0)$. The propagation matrix of the LZ transition from $-\infty$ to 0 is related to that from 0 to ∞ by Eq. (1.9). In addition to that, the LZ model with avoided crossing at the end of the pulse corresponds to Eq. (1.7) with $s(t) = \int_{T/2}^{t}\Omega'(\tau)d\tau$, which differs from the actual $s(t) = \int_0^t \Omega'(\tau)d\tau$ by $\frac{s_0}{2}$. Therefore,

$$O_{ad} = \begin{pmatrix} \alpha_{LZ}^*(k_2) & -\beta_{LZ}^*(k_2)e^{i\frac{s_0}{2}} \\ \beta_{LZ}(k_2)e^{-i\frac{s_0}{2}} & \alpha_{LZ}(k_2) \end{pmatrix}. \tag{2.1}$$

By Eq. (1.11),

$$P_{nad}(k_2, s_0) = (\alpha_{LZ}^*(k_2)\beta_{LZ}(k_2)e^{-i\frac{s_0}{2}} + \alpha_{LZ}(k_2)\beta_{LZ}^*(k_2)e^{i\frac{s_0}{2}})^2 = A(k_2)\cos^2(\frac{s_0}{2} - \phi(k_2)), \tag{2.2}$$

where

$$A(k_2) = |2\alpha_{LZ}^*(k_2)\beta_{LZ}(k_2)|^2, \quad \phi(k_2) = \arg(2\alpha_{LZ}^*(k_2)\beta_{LZ}(k_2)).$$

From Eq. (A.3),

$$2\alpha_{LZ}^*(k_2)\beta_{LZ}(k_2) = e^{-\pi k_2 + 2ik_2(1-\ln k_2)}(\frac{\pi}{\Gamma^2(\frac{1}{2} - ik_2)} + \frac{ik_2\pi}{\Gamma^2(1-ik_2)}). \tag{2.3}$$

$A(k_2)$ and $\phi(k_2)$ are the amplitude and the phase factor of the oscillation. They are plotted in Fig. 2(a). $\phi(k_2)$ increases from 0 to $\pi/2$ as k_2 varies, which explains the change from $s_0 = (2n+1)\pi$ for non-chirped inversion pulses to $s_0 = 2n\pi$ for adiabatic inversion pulses. As an example, the map of the asymptotic P_{nad} given by Eq. (2.2) is plotted in Fig. 2(b) for sinusoidal pulses. Fig. 2(b) agrees very well with Fig. 1(a) in the oscillatory region, though the nonoscillatory region is missing in Fig. 2(b).

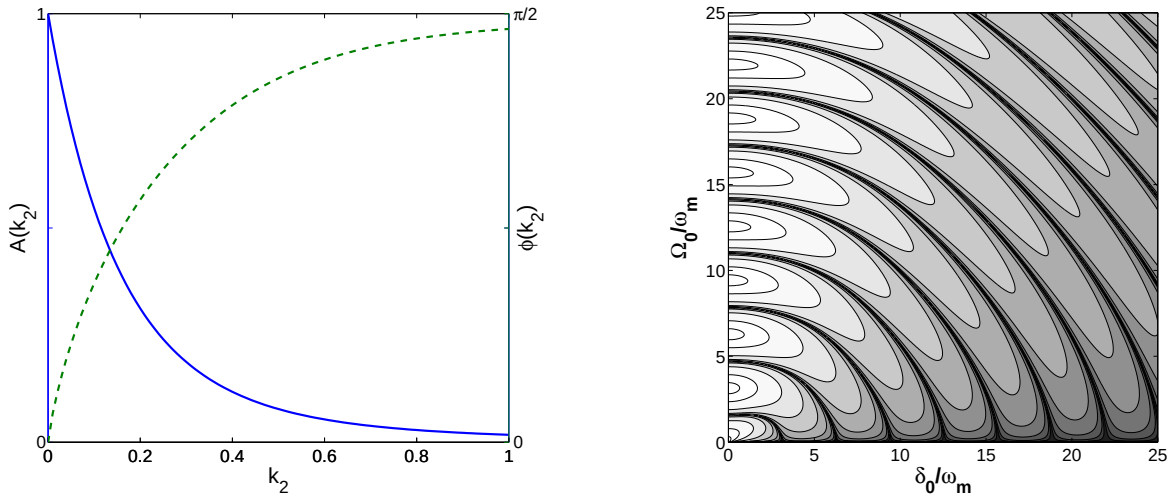

(a) Amplitude and phase factor

(b) Asymptotic P_{nad}

Figure 2: (a) Amplitude (solid line) and phase factor (dashed line) of P_{nad} in Eq. (2.2). (b) Map of P_{nad} in Eq. (2.2) for sinusoidal pulses. The curves are for $P_{nad} = 0.9, 0.5, 0.1, 0.01, 0.001, ...$

We take a closer look at Eq. (2.2) in the adiabatic limit, ie, for large k_2. Substituting the following Stirling's formulas for Gamma functions [15] into Eq. (2.3),

$$\begin{aligned}\Gamma(1-ik) &\cong \sqrt{2k\pi}\exp(-\frac{\pi k}{2}+ik(1-\ln k)-i\frac{\pi}{4})(1+\frac{i}{12k}-\frac{1}{288k^2}),\\ \Gamma(\frac{1}{2}-ik) &\cong \sqrt{2\pi}\exp(-\frac{\pi k}{2}+ik(1-\ln k))(1-\frac{i}{24k}-\frac{1}{1152k^2}),\end{aligned}$$

we have

$$2\alpha^*_{LZ}(k_2)\beta_{LZ}(k_2) \cong \frac{i}{8k_2}(1-\frac{i}{24k_2}),$$

and so

$$A(k_2) \cong (\frac{1}{8k_2})^2, \quad \phi(k_2) \cong \frac{\pi}{2}-\frac{1}{24k_2},$$

$$P_{nad} \cong (\frac{1}{8k_2})^2\sin^2(\frac{s_0}{2}+\frac{1}{24k_2}) = (\frac{\dot\Omega_0}{\delta_0^2})^2\sin^2(\frac{s_0}{2}+\frac{\dot\Omega_0}{3\delta_0^2}). \tag{2.4}$$

It agrees with the adiabatic limit Eq. (1.15) except for a phase factor of $\dot\Omega_0/(3\delta_0^2)$. To understand the discrepancy, we recall that Eq. (1.15) was obtained from first order perturbation in the rotating adiabatic frame. Higher order unitary perturbation can be obtained from the Magnus expansion [16],

$$\begin{aligned}O(t) &= \exp\Big\{-i\int_0^t dt_1 H(t_1) - \frac{1}{2}\int_0^t dt_1\int_0^{t_1} dt_2[H(t_1),H(t_2)]\\ &\quad +\frac{i}{6}\int_0^t dt_1\int_0^{t_1} dt_2\int_0^{t_2} dt_3[H(t_1),[H(t_2),H(t_3)]]+[[H(t_1),H(t_2)],H(t_3)]+\cdots\Big\}.\end{aligned} \tag{2.5}$$

Although Eq. (2.5) gives good approximation to P_{nad} over the entire parameter space [8], the computation is more complicated than the Dyson expansion [17] of the same order. To obtain the adiabatic limit of P_{nad}, it is more advantageous to use the latter. With the Hamiltonian in Eq. (1.7), the Schrödinger equation is

$$\dot\alpha(t) = \frac{\dot\theta(t)}{2}e^{-is(t)}\beta(t), \quad \dot\beta(t) = -\frac{\dot\theta(t)}{2}e^{is(t)}\alpha(t).$$

The Dyson expansion gives

$$\begin{aligned}\alpha(t) &= 1-\int_0^t dt_1\int_0^{t_1} dt_2 \frac{\dot\theta(t_2)}{2}e^{is(t_2)}\frac{\dot\theta(t_1)}{2}e^{-is(t_1)}+\cdots \\ \beta(t) &= -\int_0^t dt_1\frac{\dot\theta(t_1)}{2}e^{is(t_1)}+\int_0^t dt_1\int_0^{t_1}dt_2\int_0^{t_2}dt_3\frac{\dot\theta(t_3)}{2}e^{is(t_3)}\frac{\dot\theta(t_2)}{2}e^{-is(t_2)}\frac{\dot\theta(t_1)}{2}e^{is(t_1)}-\cdots \end{aligned} \quad (2.6)$$

In the adiabatic limit,

$$\begin{aligned}\alpha(T/2) &= 1+i\int_0^{T/2}\frac{\dot\theta^2}{4\Omega'}dt+O((\Omega_0 T)^{-2}). \\ \beta(T/2) &= -\frac{\dot\theta e^{is}}{2i\Omega'}|_0^{T/2}-[\frac{\dot\theta(T/2)e^{is(T/2)}}{\Omega'(T/2)}+\frac{\dot\theta(0)}{\Omega'(0)}]\int_0^{T/2}\frac{\dot\theta^2}{8\Omega'}dt-(\frac{e^{is}}{2\Omega'}\frac{\mathrm{d}}{\mathrm{d}t}\frac{\dot\theta}{\Omega'})|_0^{T/2}+O((\Omega_0T)^{-3}). \end{aligned} \quad (2.7)$$

Using the diabaticity defined as

$$\epsilon(t)=-\dot\theta(t)/\Omega'(t),$$

and substituting Eq. (2.7) into Eq. (1.11), we find the P_{nad} up to second order in ϵ,

$$P_{nad}\cong[\epsilon_2\sin(\frac{s_0}{2}+\int_0^{T/2}\frac{\dot\theta^2}{2\Omega'}dt+\frac{\dot\epsilon_2}{\epsilon_2\delta_0})-\frac{\dot\epsilon_1}{\Omega_0}]^2. \quad (2.8)$$

Here ϵ_1 and ϵ_2 are the diabaticity at resonance and pulse end respectively. In the region where $\epsilon_2 \gg \epsilon_1$, the avoided crossing at resonance can be neglected, and the avoided crossing at the pulse ends can be approximated by LZ transitions. Eq. (2.8) reduces to

$$P_{nad}\cong\epsilon_2^2\sin^2\left(\frac{s_0}{2}+\frac{1}{2}\int_0^\infty\frac{\delta_0^2\dot\Omega_0^2}{(\delta_0^2+\dot\Omega_0^2t^2)^{\frac{5}{2}}}dt\right)=\epsilon_2^2\sin^2\left(\frac{s_0}{2}+\frac{\epsilon_2}{2}\int_0^\infty\frac{dx}{(1+x^2)^{\frac{5}{2}}}\right)=\epsilon_2^2\sin^2(\frac{s_0}{2}+\frac{\epsilon_2}{3}).$$

It is identical to Eq. (2.4), which indicates that second order perturbation in the rotating adiabatic frame is required to obtain the asymptotic P_{nad} in Eq. (2.4).

Eq. (2.8) can be verified in another way. If the diabaticity $\epsilon(t)$ is a constant, the Hamiltonian in the adiabatic frame [8],

$$\mathcal{H}(t)=\frac{\hbar}{2}\begin{pmatrix}\Omega'(t) & i\dot\theta(t)\\ -i\dot\theta(t) & -\Omega'(t)\end{pmatrix},$$

can be integrated exactly to give

$$P_{nad}=\frac{\epsilon^2}{1+\epsilon^2}\sin^2\int_0^{T/2}\sqrt{\Omega'(t)^2+\dot\theta(t)^2}dt. \quad (2.9)$$

The particular case of sinusoidal pulses with $\Omega_0=\delta_0$ has been analyzed thoroughly in Ref. [18]. Expanding Eq. (2.9) in ϵ, we get

$$P_{nad}=\{\epsilon\sin\int_0^{T/2}(\Omega'(t)+\frac{\dot\theta(t)^2}{2\Omega'(t)})dt+O(\epsilon^3)\}^2\cong\{\epsilon\sin(\frac{s_0}{2}+\int_0^{T/2}\frac{\dot\theta^2}{2\Omega'}dt)\}^2,$$

which agrees with Eq. (2.8) as $\dot\epsilon=0$.

3 Boundary between oscillatory and nonoscillatory regions

Having studied both the nonoscillatory and oscillatory regions in the map of P_{nad} for finite chirped pulses, we will switch the focus to the boundary between the two regions, where neither the avoided crossing at

resonance nor those at the pulse ends are negligible. To take all the avoided crossings into account, we introduce a split level crossing model that combines the nonadiabatic transitions at the resonance and away from the resonance. The pulse can be decomposed into three segments, namely, before resonance, at resonance, and after resonance. Since the nonadiabatic transition probability is small in each segment, the total nonadiabatic transition *amplitude* is approximately the sum of the amplitude in each segment. At resonance, the nonadiabatic transition amplitude is determined by the LZ transition. By Eq. (A.3), the on-resonance transition amplitude is

$$A_1 = \alpha_{LZ}(k_1)\beta_{LZ}(k_1) + \alpha^*_{LZ}(k_1)\beta^*_{LZ}(k_1) = \pi e^{-\pi k_1}\left(\frac{1}{\Gamma(\frac{1}{2} - ik_1)\Gamma(\frac{1}{2} + ik_1)} - \frac{k_1}{\Gamma(1 - ik_1)\Gamma(1 + ik_1)}\right) = e^{-2\pi k_1},$$

which agrees with the nonadiabatic transition probability given in the Landau-Zener formula Eq. (1.12). The off-resonance nonadiabatic transition amplitude in the adiabatic limit was computed in Section 2. The series Eq. (2.7) would not contain the on-resonance transition amplitude $e^{-2\pi k_1}$ no matter how high the order of perturbation is, because $e^{-2\pi k_1}$ has an essential singularity at infinity, thus cannot be approximated by a power series in $1/k_1$. By Eq. (2.8), the off-resonance transition amplitude up to second order in ϵ is

$$A_2 = \epsilon_2 \sin\left(\frac{s_0}{2} + \int_0^{T/2} \frac{\dot\theta^2}{2\Omega'} dt + \frac{\dot\epsilon_2}{\epsilon_2 \delta_0}\right) - \frac{\dot\epsilon_1}{\Omega_0}.$$

Since the boundary is in the region where $\epsilon_1 \gg \epsilon_2$, A_2 can be simplified to

$$A_2 = \epsilon_2 \sin\frac{s_0}{2} - \frac{\dot\epsilon_1}{\Omega_0}.$$

As a result, the total nonadiabatic transition probability can be approximated by

$$P_{nad} \cong (A_1 + A_2)^2 = \left(e^{-2\pi k_1} + \epsilon_2 \sin\frac{s_0}{2} - \frac{\dot\epsilon_1}{\Omega_0}\right)^2. \tag{3.1}$$

To justify Eq. (3.1), we plot the traces of $P_{nad} = 0$ obtained by numerical integration against those determined by Eq. (3.1) in Fig. 3.

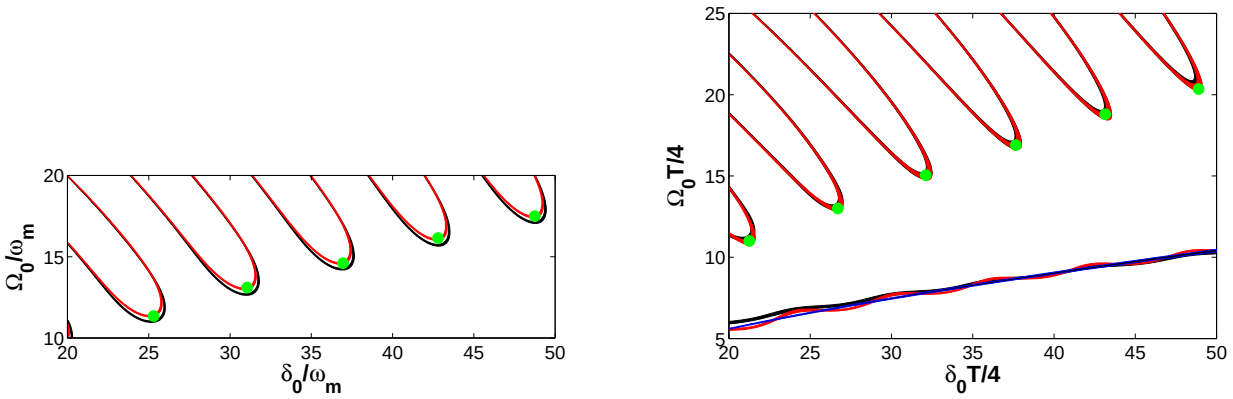

(a) Sinusoidal pulse

(b) Triangular pulse

Figure 3: (Color online) Trace of $P_{nad} = 0$ in the map along the boundary between the oscillatory and nonoscillatory regions. (a) Black curves: exact P_{nad}; red (gray) curves: approximate P_{nad} given by Eq. (3.2); dots: tips of loops given by Eq. (3.3). (b) Black curves: exact P_{nad}; red (gray) curves: approximate P_{nad} given by Eq. (3.1); lower blue (thin) curve: approximate P_{nad} given by Eq. (3.4); dots: tips of loops given by Eq. (3.5).

Fig. 3(a) is for the sinusoidal pulses. Since $\Omega(t)$ varies smoothly at resonance, $\dot\epsilon_1 = 0$. Eq. (3.1) becomes

$$P_{nad} \cong \left(e^{-2\pi k_1} + \epsilon_2 \sin\frac{s_0}{2}\right)^2. \tag{3.2}$$

The domain in Fig. 3(a) consists of large Ω_0/ω_m and δ_0/ω_m because Eq. (3.2) is only valid asymptotically. Fig. 3(a) shows that the trace of $P_{nad} = 0$ determined by Eq. (3.2) is very close to the exact trace. On the other hand, if the on-resonance transition amplitude $e^{-2\pi k_1}$ were omitted from Eq. (3.2), it would lead to a qualitatively different trace of P_{nad}, determined by $\sin s_0 = 0$, shown as the darkest regions in Fig. 2(b). To quantify the boundary between the oscillatory and nonoscillatory regions, we can define it as the envelope of the trace of $P_{nad} = 0$, connected by the "tips" of the loops, which satisfy

$$\sin\frac{s_0}{2} = -1 \Rightarrow s_0 = (4n-1)\pi \quad \text{and} \quad e^{-2\pi k_1} = \epsilon_2, \tag{3.3}$$

according to Eq. (3.2). The tips are plotted in Fig. 3(a) as well.

Fig. 3(b) plots the triangular pulses with population inversion. For triangular pulses, $\Omega(t)$ has a kink at resonance, $\dot{\epsilon}_1 = -3\epsilon_1\dot{\Omega}_1/\Omega_0 > 0$, so Eq. (3.1) has to be used. In Fig. 3(b), the trace of inversion pulses determined by Eq. (3.1) matches very well with the exact trace. Compared with sinusoidal pulses, the trace of triangular pulses with population inversion contains an extra curve below the loops. It can be explained by the difference between Eqs. (3.1) and (3.2). Eq. (3.1) has two sets of zeros. Along the lower curve, $\epsilon_2 \ll e^{-2\pi k_1}$, and the approximate equation for the trace can be simplified to

$$e^{-2\pi k_1} = \frac{\dot{\epsilon}_1}{\Omega_0}, \tag{3.4}$$

the plot of which also agrees well with the exact trace in Fig. 3(b). Along the loops, $e^{-2\pi k_1} \ll \epsilon_2$, and the trace determined by the simplified approximate equation,

$$\epsilon_2 \sin\frac{s_0}{2} = \frac{\dot{\epsilon}_1}{\Omega_0},$$

is indistinguishable from that determined by Eq. (3.1). Similarly, the boundary is defined as the envelope connected by the tips of the loops that are plotted in Fig. 3(b) and determined by

$$\sin\frac{s_0}{2} = 1 \Rightarrow s_0 = (4n+1)\pi \quad \text{and} \quad \epsilon_2 = \frac{\dot{\epsilon}_1}{\Omega_0}. \tag{3.5}$$

Equations (3.1) through (3.5) explain the qualitative difference between the traces of sinusoidal and triangular pulses with population inversion. More generally, the boundary between the oscillatory and nonoscillatory regions in the map of P_{nad} is determined asymptotically by Eq. (3.2) for smooth pulses, and Eq. (3.1) for other pulses.

4 Stable inversion pulses

In this section we will use the map of P_{nad} to design chirped pulses to achieve stable inversion of quantum state. The controlled inversion of quantum state can be used to generate large optical force on atoms in laser cooling [6] or perform the NOT operation on a qubit in quantum computing. The pulse has to achieve not only an inversion, ie, $P_{nad} = 0$, but also a stable inversion, ie, $P_{nad} < P_{th}$ as pulse parameter vary, where P_{th} is the accuracy threshold that depends on the application. In the interaction of counterpropagating light pulses with atoms, the optical force $F \propto 1 - \sqrt{P_{nad}}$ [6]. The accuracy threshold is $P_{th} = 10^{-2}$ to achieve 90% of the maximum force. Fault-tolerant quantum computation can run reliably for arbitrarily long time provided that the noise is weaker than certain accuracy threshold. In Ref. [20], it was proved that for quantum computation based on error detection and postselection, the accuracy threshold was 1.04×10^{-3}. A larger threshold allows more variation in the pulse parameters. It is well known that adiabatic pulses provide an efficient method to achieve stable inversion. We will quantify the stability in this section.

For a given pulse profile, P_{nad} depends on the coupling strength Ω_0 and detuning δ_0. In atomic experiments Ω_0 and δ_0 are stably controlled [6], so the sensitivity to δ_0 does not pose a problem. However, as

pointed out in Ref. [5], the sensitivity to Ω_0 determines the usable cross section of Gaussian laser beam. Only the portion of the cross section whose Ω_0 is within the allowed range for the accuracy threshold can be used reliably for the inversion. The energy efficiency, ie, the proportion of the usable energy, is

$$\eta = 1 - [(\Omega_0)_{min}/(\Omega_0)_{max}]^2.$$

On the other hand, the sensitivity to the Doppler shift would affect the velocity capture range of an inversion pulse. For an atom moving at velocity v, the effective detuning is shifted by $\delta_D = kv$, where k is the wave number of the resonant light.

The classical way of adiabatic inversion consists of a constant coupling strength Ω_0 and a frequency sweep from well below resonance to well above resonance. To obtain a complete inversion that is insensitive to the transition time T, $\delta_0 \gg \Omega_0$ is needed, which requires a large detuning, and thus is inefficient. Efficient methods of inversion include π-pulses and adiabatic pulses. We will compare their stability under the variation of coupling strength and Doppler shift with respect to specific accuracy thresholds.

4.1 Stability of inversion pulses

P_{nad} for π-pulses is given by Eq. (1.14). A perturbed pulse with coupling strength $\Omega_0 + \Delta\Omega$ must satisfy

$$P_{nad} = \cos^2[s_0(1 + \frac{\Delta\Omega}{\Omega_0})] = \sin^2(s_0\frac{\Delta\Omega}{\Omega_0}) < P_{th},$$

where the inversion condition $P_{nad} = \cos^2 s_0 = 0$ of the unperturbed pulse is used. For $P_{th} \ll 1$, the maximum allowed $\Delta\Omega$ is given by

$$T\Delta\Omega = C\sqrt{P_{th}}, \tag{4.1}$$

where $C = \Omega_0 T/s_0$ is a constant of order 1 depending on the pulse profile. $C = \pi$ for sinusoidal pulses, $C = 4$ for triangular pulses.

P_{nad} for adiabatic pulses is given by Eq. (1.15). The perturbed pulse must satisfy

$$P_{nad} \approx \epsilon_2^2 \sin^2(s_0 + \frac{\partial s_0}{\partial\Omega_0}\Delta\Omega) < P_{th},$$

where s_0 is regarded as a function of δ_0 and Ω_0. Using the inversion condition $P_{nad} = \epsilon_2^2 \sin^2 s_0 = 0$ of the unperturbed pulse, we obtain the maximum allowed $\Delta\Omega$ for $P_{th} \ll 1$,

$$\Delta\Omega = C\frac{\delta_0^2}{\Omega_0}\sqrt{P_{th}}, \tag{4.2}$$

where $C = (\Omega_0/\dot{\Omega}_0)(\partial\Omega_0/\partial s_0)$ is a number of order 1 depending on the pulse profile and parameters. By comparing Eqs. (4.1) and (4.2), the allowed $\Delta\Omega$ for adiabatic pulses with $\epsilon_2 \ll 1$ is much larger than that for π-pulses under the same threshold. Among adiabatic pulses, the pulses with larger δ_0 and smaller Ω_0 are preferred in order to allow larger $\Delta\Omega$.

The profiles of the π-pulse and the adiabatical pulse with Doppler shift are plotted in Fig. 4. For a Doppler-shifted π-pulse,

$$\alpha(T/2) = \alpha_{LZ}(k_2), \quad \beta(T/2) = \beta^*_{LZ}(k_2)e^{is'_0}, \quad \alpha(-T/2) = \alpha_{LZ}(k_2), \quad \beta(-T/2) = -\beta_{LZ}(k_2)e^{-is'_0},$$

where $k_2 = \delta_D^2/(8\dot{\Omega}_0)$ is the adiabaticity at the two ends of the doppler-shifted pulse, and

$$s'_0 = \frac{1}{2}\int_{-T/2}^{T/2}\sqrt{\Omega^2(t) + (\delta(t) - \delta_D)^2}dt. \tag{4.3}$$

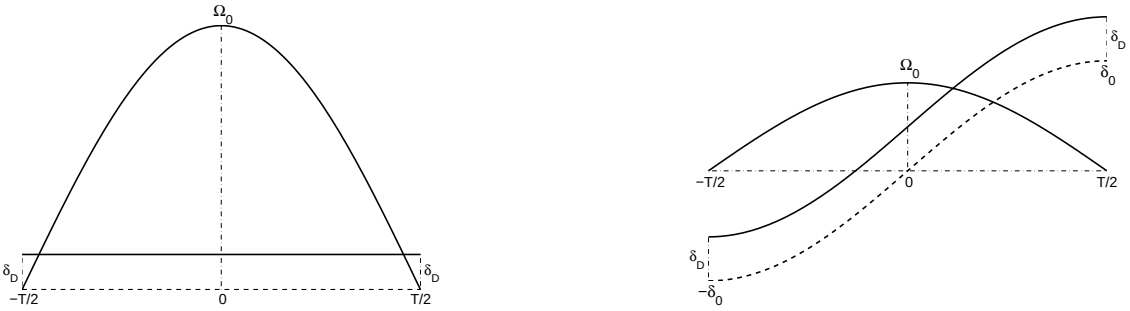

(a) π-pulse

(b) Adiabatic pulse

Figure 4: Profiles of Doppler-shifted pulses. Dashed lines are the detuning without Doppler shift.

Since the adiabatic states at the end of the pulse are the *same* as those at the beginning of the pulse,

$$P_{nad} = |\alpha_{ad}|^2 = |\alpha_{LZ}^2(k_2) + \beta_{LZ}^2(k_2)e^{-2is_0'}|^2.$$

Using the inversion condition $P_{nad} = \cos^2 s_0 = 0$, the fact that $s_0' - s_0$ is of the order of k_2, and the asymptotic forms of $\alpha_{LZ}(k_2)$ and $\beta_{LZ}(k_2)$ obtained from Eq. (A.3), we have for $k_2 \ll 1$,

$$P_{nad} = |\alpha_{LZ}^2(k_2) - \beta_{LZ}^2(k_2)|^2 = 2\pi k_2 < P_{th}.$$

Therefore the maximum allowed Doppler shift is

$$\delta_D = \sqrt{\frac{4}{\pi}\dot{\Omega}_0 P_{th}}. \tag{4.4}$$

For a Doppler-shifted adiabatic pulse, the perturbation method in the rotating adiabatic frame still applies, except that the detuning is no longer symmetric. By the first order approximation,

$$P_{nad} = \left| \frac{\epsilon(t)e^{is(t)}}{2i} \right|_{-T/2}^{T/2} \Bigg|^2 = (\frac{\epsilon_+ + \epsilon_-}{2} \sin s_0')^2 + (\frac{\epsilon_+ - \epsilon_-}{2} \cos s_0')^2,$$

where $\epsilon_\pm = \dot{\Omega}_0/(\delta_0 \pm \delta_D)^2$ are the diabaticity at the two ends of the Doppler-shifted pulse, and s_0' is defined by Eq. (4.3). Using the inversion condition $P_{nad} = \epsilon_2^2 \sin^2 s_0 = 0$ and the fact that $s_0' - s_0$ is of the order of $T\delta_D^2/\delta_0$, we have for $\delta_D \ll \delta_0$,

$$P_{nad} = (2\epsilon_2 \frac{\delta_D}{\delta_0})^2 < P_{th}.$$

The maximum allowed Doppler shift is given by

$$\frac{\delta_D}{\delta_0} = \frac{\delta_0^2}{\dot{\Omega}_0} \frac{\sqrt{P_{th}}}{2}. \tag{4.5}$$

By comparing Eqs. (4.4) and (4.5), adiabatic pulses have larger velocity capture range than π-pulses. Among adiabatic pulses, the pulses with larger δ_0 and smaller Ω_0 are also preferred for larger velocity capture range.

4.2 Examples of stable inversion pulses

We present and compare a few sinusoidal inversion pulses with small coupling strength and detuning. The pulses are shown in the magnified map of P_{nad} for sinusoidal pulses Fig. 5(a). Point A represents the first

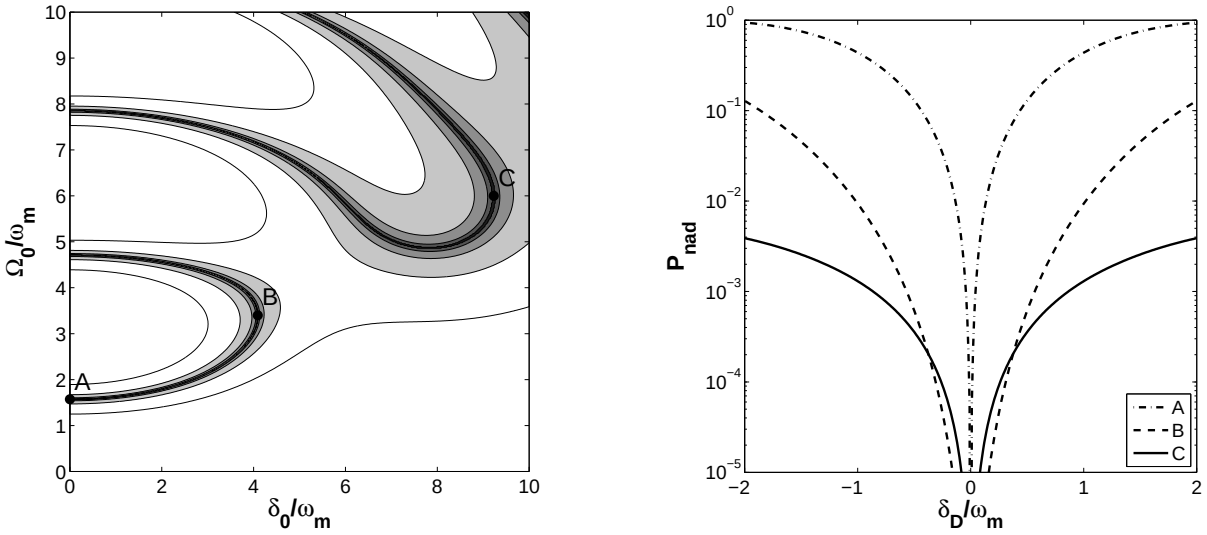

(a) P_{nad} (b) Doppler shift

Figure 5: (a) Magnified map of P_{nad} for sinusoidal pulses. The curves are for $P_{nad} = 0.1, 0.01, 0.001, ...$ Point A is the π-pulse, points B and C are the adiabatic pulses. (b) P_{nad} with Doppler shift for the points A, B and C.

π-pulse, whose $\delta_0 = 0$ and $s_0 = \pi/2$. Points B and C represent two adiabatic pulses, chosen as the pulses with the largest detuning on the first and second "loops" in the map. P_{nad} for each pulse is plotted against the Doppler shift in Fig. 5(b). The maximum allowed deviation in the coupling strength, the corresponding energy efficiency, and the maximum allowed Doppler shift are listed in Table 1 for each pulse, with respect to the accuracy threshold 10^{-3} and 10^{-2}.

	$P_{nad} < 10^{-3}$			$P_{nad} < 10^{-2}$		
Pulse parameters	$\Delta\Omega_0$	η	δ_D	$\Delta\Omega_0$	η	δ_D
A ($\delta_0 = 0, \Omega_0 = \pi/2$)	0.032	7.8%	0.043	0.100	22.5%	0.135
B ($\delta_0 = 4.1, \Omega_0 = 3.4$)	0.425	40%	0.57	0.775	60%	1.02
C ($\delta_0 = 9.2, \Omega_0 = 6.0$)	0.954	50%	0.86	2.055	75%	4.65

Table 1: Maximum allowed deviation in coupling strength, energy efficiency, and maximum allowed Doppler shift of the sinusoidal pulses with respect to the accuracy threshold. All frequencies are in the unit of ω_m.

In Table 1, $\Delta\Omega$ and δ_D for the π-pulse agree well with Eqs. (4.1) and (4.4). $\Delta\Omega$ and δ_D for the adiabatic pulses agree with Eqs. (4.1) and (4.4) only qualitatively because the pulses are close to the boundary between the oscillatory and nonoscillatory regions in the map, where P_{nad} need to be approximated by the more complicated Eq. (3.1). According to Table 1, $\Delta\Omega_0$ for the threshold $P_{th} = 10^{-3}$ is more than 10 times bigger for the adiabatic pulses than for the π-pulse, and the energy efficiency is more than 5 times higher. The energy efficiency is further boosted by half for the more relaxed accuracy threshold $P_{th} = 10^{-2}$. The adiabatic pulses allow 10 times bigger Doppler shifts than the π-pulse for the same accuracy threshold. It is in contrast to the half adiabatic pulse with constant adiabaticity in Ref. [5], because at the two ends the sinusoidal pulses have detuning $\pm\delta_0$, while the pulses in Ref. [5] have vanishingly small detuning.

Similar adiabatic pulses can be selected from the map of P_{nad} for triangular pulses Fig. 1(b). For a generic pulse profile, which may be neither sinusoidal nor triangular [6], an adiabatic inversion pulse with relatively small coupling strength and detuning can be selected from the corresponding map of P_{nad}, with

guidance by Eqs. (4.2) and (4.5). The adiabatic pulse has higher power efficiency and larger velocity capture range than the π-pulse.

5 Conclusion

We studied the map of the nonadiabatic transition probability P_{nad} in the parameter space of the coupling strength and detuning amplitude for chirped pulses. The oscillation of P_{nad} is due to the interference of the nonadiabatic transitions at the beginning and the end of the pulse. The boundary between the oscillatory and nonoscillatory regions of the map is formed by the interference between the on-resonance transition and off-resonance transition. The map of P_{nad} can aid the design of efficient chirped pulses to achieve stable population inversion. We proved that adiabatic pulses with larger detuning amplitude and smaller coupling strength are optimal both for high power efficiency and for large velocity capture range. Finally, as pointed out by Vitanov and Garraway [4], P_{nad} only depends on the function $\theta(s)$. Therefore the sinusoidal or triangular pulses described in this paper can be generalized to fit a specified coupling or detuning profile without altering the transition probability.

Acknowledgements

Author is grateful to the referee for useful advices and references. This work is supported by the Kansas NSF EPSCoR First Award.

A Landau-Zener transition in the rotating adiabatic frame

The Landau-Zener model defined by Eqs. (1.1) and (1.2) is well-known to be analytically solvable. For the applicability in Section 2, we derive the propagation matrix from 0 to ∞ rather than from $-\infty$ to ∞ as in most literatures. Following Zener's paper [2], we write the wave function as

$$\psi(t) = e^{-i\frac{at^2}{4}} c_+(t)\psi_+ + e^{i\frac{at^2}{4}} c_-(t)\psi_-.$$

$c_+(t)$ satisfies the following equation,

$$\frac{\mathrm{d}^2 c_+}{\mathrm{d}t^2} - iat\frac{\mathrm{d}c_+}{\mathrm{d}t} + \frac{b^2}{4}c_+ = 0.$$

Letting $z = iat^2/2$, we can convert the equation above to the Kummer's equation,

$$z\frac{\mathrm{d}^2 c_+}{\mathrm{d}z^2} + (\frac{1}{2} - z)\frac{\mathrm{d}c_+}{\mathrm{d}z} - \frac{ib^2}{8a}c_+ = 0.$$

The solution is

$$c_+(t) = F\left(i\frac{b^2}{8a}; \frac{1}{2}; i\frac{at^2}{2}\right) c_+(0) - i\frac{bt}{2}F\left(i\frac{b^2}{8a} + \frac{1}{2}; \frac{3}{2}; i\frac{at^2}{2}\right) c_-(0). \tag{A.1}$$

where F is the confluent hypergeometric function [15]. Consequently, the propagation matrix from 0 to t is

$$O_0(t) = \begin{pmatrix} e^{-i\frac{at^2}{4}} F\left(i\frac{b^2}{8a}; \frac{1}{2}; i\frac{at^2}{2}\right) & -i\frac{bt}{2}e^{-i\frac{at^2}{4}} F\left(i\frac{b^2}{8a} + \frac{1}{2}; \frac{3}{2}; i\frac{at^2}{2}\right) \\ -i\frac{bt}{2}e^{i\frac{at^2}{4}} F\left(-i\frac{b^2}{8a} + \frac{1}{2}; \frac{3}{2}; -i\frac{at^2}{2}\right) & e^{i\frac{at^2}{4}} F\left(-i\frac{b^2}{8a}; \frac{1}{2}; -i\frac{at^2}{2}\right) \end{pmatrix}.$$

As $t \to \infty$, $O_0(t)$ does not converge because of the highly oscillating phases. However, the propagation matrix in the rotating adiabatic frame converges as $t \to \infty$ because the oscillating phases are cancelled by the phases in the eigenstates. The quantum state in the rotating adiabatic frame is associated with the state in the original frame by [8]

$$\psi(t) = U(t)\psi_0(t) = \begin{pmatrix} \exp(i\frac{s(t)}{2}) & 0 \\ 0 & \exp(-i\frac{s(t)}{2}) \end{pmatrix} \begin{pmatrix} \cos(\frac{\theta(t)}{2}) & \sin(\frac{\theta(t)}{2}) \\ -\sin(\frac{\theta(t)}{2}) & \cos(\frac{\theta(t)}{2}) \end{pmatrix} \psi_0(t), \tag{A.2}$$

in which $\theta(t)$ and $s(t)$ are defined after Eq. (1.7), with $\Omega(t)$ and $\delta(t)$ given in Eq. (1.2). As $t \to \infty$, the propagation matrix in the rotating adiabatic frame, denoted by O_{LZ}, becomes

$$\begin{aligned} O_{LZ}(\infty) &= \lim_{t\to\infty} U(t)O_0(t)U^\dagger(0) \\ &= \lim_{t\to\infty} \begin{pmatrix} \exp(\frac{i}{2}\int_0^t \sqrt{b^2+(a\tau)^2}d\tau) & 0 \\ 0 & \exp(-\frac{i}{2}\int_0^t \sqrt{b^2+(a\tau)^2}d\tau) \end{pmatrix} O_0(t) \begin{pmatrix} \frac{\sqrt{2}}{2} & -\frac{\sqrt{2}}{2} \\ \frac{\sqrt{2}}{2} & \frac{\sqrt{2}}{2} \end{pmatrix} \\ &= e^{-\frac{\pi}{2}k} \begin{pmatrix} e^{ik(1-\ln k)}\frac{\Gamma(\frac{1}{2})}{\Gamma(\frac{1}{2}-ik)} & e^{ik(1-\ln k)-i\frac{\pi}{4}}\sqrt{k}\frac{\Gamma(\frac{1}{2})}{\Gamma(1-ik)} \\ -e^{-ik(1-\ln k)+i\frac{\pi}{4}}\sqrt{k}\frac{\Gamma(\frac{1}{2})}{\Gamma(1+ik)} & e^{-ik(1-\ln k)}\frac{\Gamma(\frac{1}{2})}{\Gamma(\frac{1}{2}+ik)} \end{pmatrix} \begin{pmatrix} \frac{\sqrt{2}}{2} & -\frac{\sqrt{2}}{2} \\ \frac{\sqrt{2}}{2} & \frac{\sqrt{2}}{2} \end{pmatrix}, \end{aligned}$$

where $k = b^2/(8a)$ is the adiabaticity at the avoided crossing. The asymptotic form of the confluent hypergeometric function [15] has been used in the derivation of the last equality. Substituting $O_{LZ}(\infty)$ into Eq. (1.8), we obtain the coefficients α and β for the Landau-Zener model in the limit that $t \to \infty$ as functions of k,

$$\begin{aligned} \alpha_{LZ}(k) &= \sqrt{\frac{\pi}{2}} \exp\Big\{-\frac{\pi}{2}k - ik(1-\ln k)\Big\} \left[\frac{1}{\Gamma(\frac{1}{2}+ik)} + e^{i\frac{\pi}{4}}\frac{\sqrt{k}}{\Gamma(1+ik)}\right], \\ \beta_{LZ}(k) &= \sqrt{\frac{\pi}{2}} \exp\Big\{-\frac{\pi}{2}k + ik(1-\ln k)\Big\} \left[\frac{1}{\Gamma(\frac{1}{2}-ik)} - e^{-i\frac{\pi}{4}}\frac{\sqrt{k}}{\Gamma(1-ik)}\right]. \end{aligned} \tag{A.3}$$

It recovers the half crossing transition probability [21], $P = |\alpha_{LZ} - \beta^*_{LZ}|^2/2 = (1 - e^{-2\pi k})/2$.

References

[1] L. Landau, *Phys. Z. Sowjetunion* **2**, 46 (1932).

[2] C. Zener, *Proc. R. Soc. London, Ser. A* **137**, 696 (1932).

[3] A. Abragam, The Principles of Nuclear Magnetism, Section II.E.(c), Clarendon, Oxford (1961).

[4] N. V. Vitanov and B. M. Garraway, *Phys. Rev. A* **53**, 4288 (1996).

[5] J. Bateman and T. Freegarde, *Phys. Rev. A* **76**, 013416 (2007).

[6] X. Miao, E. Wertz, M. G. Cohen and H. Metcalf, *Phys. Rev. A* **75**, 011402 (2007).

[7] T. Lu, X. Miao and H. Metcalf, *Phys. Rev. A* **71**, 061405 (2005).

[8] T. Lu, X. Miao and H. Metcalf, *Phys. Rev. A* **75**, 063422 (2007).

[9] Yu. N. Demkov and M. Kunike, *Vestn. Leningr. Univ. Fis. Khim.* **16**, 39 (1969).

[10] M. V. Berry, *Proc. R. Soc. London A* **429**, 61 (1990).

[11] L. Allen and J. H. Eberly, Optical Resonance and Two-Level atoms, Dover (1987).

[12] A. M. Dykhne, *Sov. Phys. JETP* **11**, 411 (1960).

[13] J. P. Davis and P. Pechukas, *J. Chem. Phys.* **64**, 3129 (1976).

[14] K.-A. Suominen, B. M. Garraway and S. Stenholm, *Optics Comm.* **82**, 260 (1991).

[15] M. Abramowitz and I. A. Stegun, Handbook of Mathematical Functions, Dover (1964).

[16] W. Magnus, *Comm. Pure and Appl. Math.* **7**, 649 (1954).

[17] J. J. Sakurai, Modern Quantum Mechanics, Sect. 5.6, Addison-Wesley (1994).

[18] D. Sawicki and J. H. Eberly, *Optics Express* **4**, 217 (1999).

[19] K.-A. Suominen and B. M. Garraway, *Phys. Rev. A* **45**, 374 (1992).

[20] P. Aliferis, D. Gottesman and J. Preskill, *Quant. Inf. Comput.* **8**, 181 (2008).

[21] C. E. Carroll and F. T. Hioe, *J. Phys. A* **19**, 2061 (1986).